A&A 488, 559–564 (2008)
DOI: 10.1051/0004-6361:200809952

Astronomy & Astrophysics

An upper limit of gaseous water abundance in Chamaeleon-MMS1 as observed with ODIN⋆

A. Klotz[1], J. Harju[2], I. Ristorcelli[1], M. Juvela[2], N. Boudet[1], and L. K. Haikala[2]

[1] CESR, Observatoire Midi-Pyrénées (CNRS-UPS), Université de Toulouse, BP 4346, 31028 Toulouse Cedex 04, France
e-mail: klotz@cesr.fr
[2] Observatory, PO Box 14, 00014 University of Helsinki, Finland

Received 11 April 2008 / Accepted 14 May 2008

ABSTRACT

Context. The determination of the gaseous water abundances in different intestellar environments is crucial for understanding the oxygen chemistry and its role in the molecular cloud evolution.
Aims. The purpose of this study is to estimate water abundance in the protostellar core Cha-MMS1.
Methods. The ground-state line of o-H_20 at 557 GHz was observed with the ODIN telescope. Two observing runs performed in 2002 and 2003 resulted in an upper limit of T_A = 16 mK. A model for the core density and temperature structure was constructed using a 1.3 mm continuum map from SEST/SIMBA. The water abundance profile through the cloud was derived and water line intensities expected from this model were calculated.
Results. An upper limit of 7×10^{-9} was derived for the average fractional o-H_2O abundance (relative to H_2). The non-detection is consistent with an abundance profile where a high fractional abundance ($\sim 10^{-7}$) is reached in the low-density envelope of the core. According to our radiative transfer calculations, the detection of the 557 GHz line from a quiescent core should severely be hampered by self-absorption. Therefore the present observations do not put hard contrainst on the H_2O abundance.

Key words. ISM: clouds – ISM: individual objects: Chamaeleon-MMS1 – ISM: abundances – stars: formation

1. Introduction

The study of water abundance is of particular interest in star forming regions because of its potential key role both in the thermal balance and chemical evolution of the molecular dense clouds. It has long been expected from steady-state gas phase models that H_2O and O_2, along with O and CO, are the gas-phase reservoirs of oxygen (e.g. Lee et al. 1996; Bergin et al. 1996; Millar 1997) and the main coolants of the dense gas (e.g. Goldsmith & Langer 1978; Hollenbach 1988; Neufeld et al. 1995). The satellite observations of SWAS, ISO and more recently Odin, in a large variety of astronomical objects, have put hard constraints on these chemical models. The abundance of gaseous H_2O shows significant variations from one medium to another. It can reach a few $10^{-5}/H_2$ in the warm gas of protostellar envelope and outflows ($T \geq 300$ K, $n(H_2) \geq 10^3$ cm^{-3}), in agreement with model predictions (e.g. Harwit et al. 1998; Giannini et al. 2001; Melnick et al. 2000; Neufeld et al. 2000; Franklin et al. 2007), and decrease down to very low values, 100 to 1000 times below the predictions, in the cold and dense molecular clouds (Bergin et al. 2000; Snell et al. 2000a–c).

According to the current picture, water is produced efficiently in the gas phase through ion-molecule reactions as long as atomic oxygen is present. Close to cloud surfaces water molecules are destroyed in photodissociation by UV radiation (e.g. Spaans & van Dishoeck 2001). On the other hand, deep in the cloud the gas-phase water abundance is reduced because of the adsorption of H_2O molecules or O atoms onto grain surfaces (e.g. Bergin & Melnick 2005). Once condensed, water is likely to remain frozen on the grain surfaces during most part of the evolution of a dense low-mass core. It seems possible though that during this phase gaseous water can be found in a layer with moderate extinctions where H_2O formation and destruction are in balance (see e.g. Bergin & Snell 2002; Bergin & Melnick 2005).

Very young protostars disturb the surrounding core by high velocity jets which give rise to shocks and outflows. Shocks heating the grains above 100 K can release water into the gas phase. Water abundance can be greatly increased at still higher temperatures when neutral-neutral reactions become efficient. Dense cores embedding Class 0 or Class I protostars are therefore prospective targets for detecting gaseous water.

The ground-state rotational line (1_{10}–1_{01}) of ortho-H_2O at 557 GHz which was accessible to the Odin and SWAS satellites provides an opportunity to detect thermally excited water in cool gas. The critical density of this line is 3×10^8 cm^{-3} (Hjalmarson et al. 2003), and the upper state energy is only 27 K.

In this paper we report on Odin measurements of ortho-H_2O at 557 GHz towards the dense molecular core Cha-MMS1 which has been suggested to contain a protostar at a very early stage of evolution. In the following section we present a summary of previous observational data on Cha-MMS1. The present

⋆ Based on observations with Odin, a Swedish-led satellite project funded jointly by the Swedish National Space Board (SNSB), the Canadian Space Agency (CSA), the National Technology Agency of Finland (Tekes) and Centre National d'Étude Spatiale (CNES). The Swedish Space Corporation has been the industrial prime contractor and also is operating the satellite. Complementary data were collected at the European Southern Observatory, La Silla, Chile.

Table 1. Set-up of ODIN runs on Cha-MMS1.

Backend	Date start	Date end	Integ. Time	Noise rms (Ta)	$\alpha_{J2000,0}$	$\delta_{J2000,0}$
AOS	2002–07–16.8	2002–07–21.5	44×10^3 s	19 mK	$11^h06^h37\overset{s}{.}2 \pm 1\overset{s}{.}2$	$-77°23'53'' \pm 7''$
AC2	2003–01–18.5	2003–01–19.4	14×10^3 s	38 mK	$11^h06^h21\overset{s}{.}0 \pm 0\overset{s}{.}4$	$-77°23'00'' \pm 4''$

The coordinates of the beam centres and their errors are given in the two last columns. The errors correspond to the spacecraft attitude errors caused mainly by non-corrected stellar aberration (see Frisk et al. 2003, for details).

observations and data processing are described in Sects. 3 and 4. In Sect. 5, we derive an upper limit of the water abundance.

2. The Cha-MMS1 core

The Chamaeleon I dark cloud (Cha I) is a nearby star forming region with a distance of about 150 pc (Knude & Høg 1998). Recent summaries of the cloud properties and its stellar population can be found in Bally et al. (2006) and Haikala et al. (2005).

The compact thermal dust emission source Cha-MMS1 (Reipurth et al. 1996) lies in the vicinity of the Cederblad 110 reflection nebula in the central part of the Cha I cloud. The object is associated with a small group of young stellar objects. The nearest neighbours are the Class I protostar IRS4 (Prusti et al. 1991; Zinnecker et al. 1999; Persi et al. 2001) some 1.′3 NE, and the young brown dwarf candidate NIR89 (Persi et al. 2001) about 1.′3 east of the dust continuum peak Cha-MMS1a. The coordinates of Cha-MMS1a are $\alpha_{J2000,0} = 11^h06^m31\overset{s}{.}7$, $\delta_{J2000,0} = -77°23'32''$. A molecular outflow was detected in the vicinity of Cha-MMS1 (Mattila et al. 1989; Prusti et al. 1991).

Submillimetre molecular lines from the Cha-MMS1 core were recently observed by Belloche et al. (2006). This paper presents a comprehensive analysis of the nature of the core, and gives an overview of previous molecular line and continuum studies of the region. The chemical properties of the core have been also discussed by Kontinen et al. (2000) and Tennekes et al. (2006). The main conclusion of Belloche et al. (2006) is that Cha-MMS1 is not powering the molecular outflow and that it therefore represents either a prestellar core or a transitional object between the prestellar and Class 0 stages. The density distribution assumed by Belloche et al. (2006) has a flat inner region ($n(H_2) \sim 3.3 \times 10^6$ cm^{-3} within a radius of 1800 AU or 12″), and a thin outer shell with $n(H_2) \propto r^{-2}$ up to 2400 AU (16″). In agreement with the assumption of a very dense core without an internal heating source, the chemistry of this object is characterized by a large N_2D^+/N_2H^+ abundance ratio, a lower DCO^+/HCO^+ abundance ratio (reflecting CO depletion in the densest part), and a detectable abundance of H_2D^+.

Using the CO(3–2) line, Belloche et al. (2006) could locate the centre of the molecular outflow. It seems now very likely that the outflow is powered by IRS4, and not by Cha-MMS1 as suggested by Reipurth et al. (1996), and more recently by Bally et al. (2006). On the other hand, from the CO(3–2) map it seems possible that the blueshifted outflow interacts with the Cha-MMS1 core. Hiramatsu et al. (2007) came to a similar conclusion, and suggested furthermore that the outflow from IRS4 may have affected substantially the core dynamics.

3. Observations

3.1. Odin

ODIN satellite is a 1.1 m space telescope devoted to high resolution submillimeter spectroscopy (Frisk et al. 2003). Back-end spectrometers consist of an acousto-optical spectrometer (AOS) and two autocorrelators (AC1 and AC2). There are two observing modes involving on/off measurements (Olberg et al. 2003): *Dicke-switching* using an *off* position 42° away from the target, and *position switching* where the telescope pointing is alternated between the target and a nearby *off* position (typically 2.5° away) about once per minute.

We performed two observing runs with ODIN to obtain spectra of the ortho-$H_2^{16}O$ (1_{10}–1_{01}) line at 556 936 MHz. At this frequency the beam size is 2.1 arcmin. Table 1 summarizes parameters and results of the two runs. The bandwidths of the spectrometers used for H_2O observations were ~1000 MHz, and the channel width was 1 MHz. For data access, we used the SGDO (Système de Gestion des Données Odin) at CNES. This system archives all the level 0 data from ODIN and processes them automatically to provide level 1b data for users. This system is independent of the PDC (Parallel Data Center) in Stockholm which stores also level 0 data but does not deliver ready-to-use level 1b data. A level 1b data file downloaded from SGDO contains all calibrated scans acquired during one orbit. We have extracted scans on the sky (i.e. outside the Earth occultation) and corrected them for the Doppler shift due to the orbital motion of the satellite using IDL scripts developed by Baron (private communication). We identified the off and target position scans, and averaged them to obtain a single spectrum per run. Spectra are displayed in Fig. 2. The celestial position of the beam center was calculated using ACS align parameters provided by the ODIN team corresponding to the range of dates of our observations. To verify our data processing scripts, we processed data of the source W3 published by Wilson et al. (2003). We obtained the same results.

The 2002 run was carried out in the *Dicke switching* mode using the AOS. The pointing was shifted by 27 arcsec South-East of the centre of Cha-MMS1. No line is detected above an rms noise of 19 mK. The 2003 run was much shorter than that in 2002. It was carried out in the *Dicke switching* mode using AC2. This time the pointing was shifted by 48″ North-West of the aimed position. The rms noise level reached during this run 38 mK. The intersection of the 2002 and 2003 beams cover the central part of Cha-MMS1. Combining the 2002 and 2003 data, we have no detection down to a level of 16 mK (rms).

3.2. SIMBA

The millimeter continuum observations were carried out on Nov. 11th and 23rd, 2001 with the 37 channel SEST bolometer array, SIMBA. The central frequency of this instrument is 250 GHz and the band width is about 50 GHz. The HPBW of a single bolometer element is ~24″. Frequent skydips were used to determine the atmospheric opacity and the values obtained were from 0.25 to 0.29 and 0.18 during the Nov. 11th and 23rd observations, respectively. Pointing was controlled by observing sources with known accurate coordinates and is estimated to be

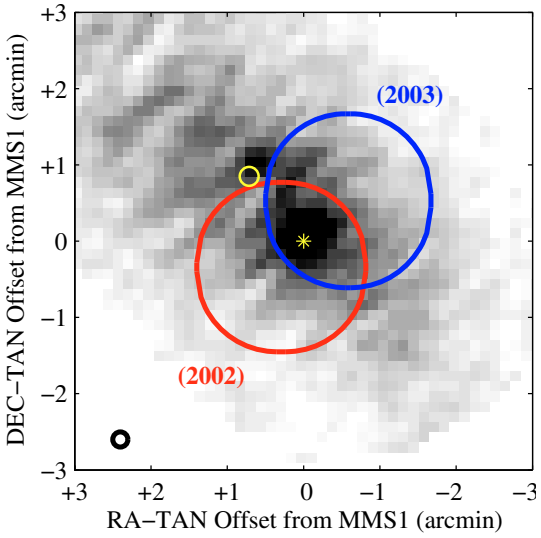

Fig. 1. The positions of the ODIN beam during the two runs superposed on the 1.3 mm continuum map. The SIMBA beam is 24″ (black circle near the *left-bottom corner*). The location of the continuum peak Cha-MMS1a is indicated with a star. Its coordinates are $\alpha_{J2000,0} = 11^h06^m31\overset{s}{.}7$, $\delta_{J2000,0} = -77°23'32''$. The YSO IRS4 is marked with a circle.

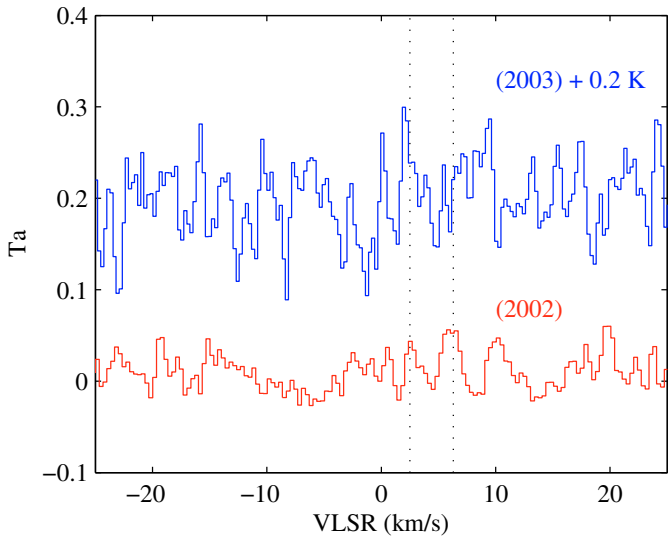

Fig. 2. Spectra of the two ODIN runs on Cha-MMS1 centered on the frequency of the ortho-$H_2^{16}O$ (1_{10}–1_{01}) line (see details in Table 1). The dashed lines indicate the v_{LSR} range in which molecular lines are usually found towards this source (cf. Sect. 2).

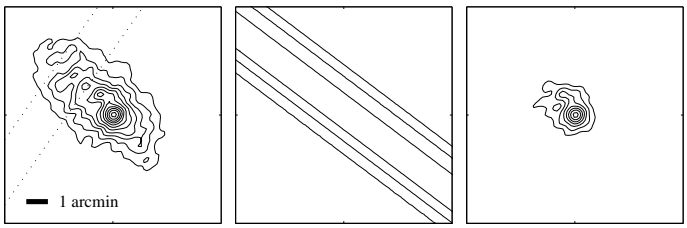

Fig. 3. Separation process to substract the contribution of the extended envelope from the emission of the Cha-MMS1 core. Contours are plotted every 2 MJy/sr. The angular scale is indicated by a 1′ bar. *Left*: the original image. The dashed lines indicate the region used to calculate the median profile. *Middle*: the median map of the diffuse envelope, assuming the median profile derived from the left panel expanded along the major axis of the envelope. *Right*: the Cha-MMS1 core after the substraction of the synthetized diffuse envelope.

better than 10″. Uranus was used to obtain calibration. The observations were done in the fast-scanning mode with a scanning speed of 80″/s in azimuth. The maps consisted of 81 scans each 900″ long in azimuth spaced by 8″ in elevation.

The data was reduced using the MOPSIC[1] data reduction package as explained in Miettinen et al. (2006). The size of the SIMBA array on sky is ∼4′. The observing mode restricts the maximum extent of the detectable surface emission to the array size in the sky. Sensitivity fluctuations result in artefacts in the scanning direction.

The observed distribution of the 1.2 mm continuum emission in the direction of Cha-MMS1 is presented in Fig. 1. Both Cha-MMS1 (the stronger source in the figure) and IRS 4 are seen in the map. The two sources are seen projected on elongated surface emission. Because the instrument cannot detect structures larger than the array size, the level of the extended emission is a lower limit. The maximum intensity in the direction of Cha-MMS1 is 378 mJy/beam (25.6 MJy/sr), in very good agreement with the value 370 mJy/beam measured by Reipurth et al. (1996).

4. Component separation

The 1.3 mm surface brightness map from SIMBA was used to construct a model for the density distribution in the vicinity of Cha-MMS1. We identified three components on the map: i) the Cha-MMS1 core itself, ii) the circumstellar envelope around IRS4, and iii) an extended envelope. The distribution of the extended envelope can be approximated by an ellipse of axes 4.0 × 7.3′ at a 2 MJy/sr level, centered near IRS4. The major axis is tilted by ∼55° from the North. The extended component reaches about 7 MJy/sr close to the positions of Cha-MMS1 and IRS 4. This intensity corresponds to about 25% of the peak brightness towards Cha-MMS1.

Cha-MMS1 lies close to the major axis of the extended envelope. In the neighbourhood of the core, the iso–intensity contours lie approximately parallel with the major axis of the envelope. We used this property in the subtraction of the diffuse component. The method is illustrated in Fig. 3. We first constructed a synthetic image of the diffuse emission (Fig. 3 middle panel) as an expansion of the median profile in a window (1.′8 in width) across the extended envelope (dashed lines in Fig. 3 left). After the substraction of the synthetic extended component, we obtained an image with Cha-MMS1 and IRS4 separated from the background (Fig. 3 right).

The brightness profile of Cha-MMS1 was synthesized by averaging the intensity on concentric circular rings. We used a polar projection to perform this procedure. This method makes it possible to suppress the contributions of IRS4 and striping to the image. Figure 4 show the two separated components. The core is found to extend to a radial distance of ∼170″ from the centre.

5. Core model and water abundance

We used the core emission component separated in the previous section to construct a model for the density and temperature structure of Cha-MMS1. This was performed by modelling the surface brightness distribution assuming a "flat top + powerlaw" ($\sim r^p$) density profile. The temperature gradient due to

[1] MOPSIC is a software package for infrared, millimeter and radio data reduction developed and upgraded by Zylka.

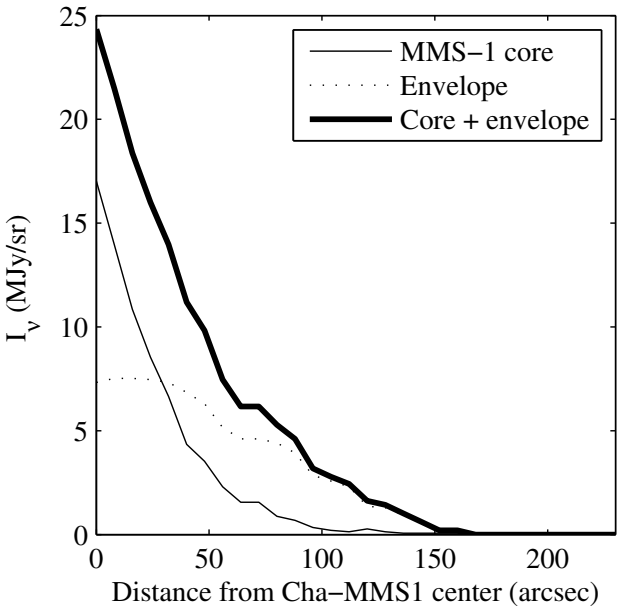

Fig. 4. The brightness emission profiles derived from the extraction method described in Sect. 4.

attenuation of the ISRF was taken into account, but the dust temperature was not allowed to go below 7 K in the core centre. The observed surface brightness was fitted inside 170″. A pedestal of 2 MJy/sr was added to the SIMBA values. This corresponds to the surface brightness at the outer boundaries of the extended envelope. The addition was done because of two reasons: 1) the SIMBA map does not necessarily contain all the large scale emission (see Sect. 6), and 2) it is otherwise not possible to fit the density with a powerlaw. The model was extended to 230″ (see Fig. 4) so that it would contain a region where the A_V drops below 2, i.e., to the outer region where the water abundance should drop because of photodissociation. The observed brightness emission profile (Fig. 4) can be fitted by a model in which the density profile has different exponent inside and outside the radius of 90″. In this model, the inner profile has $p = -1.6$, and the outer has $p = -3.7$. The central constant density region has a radius of 13.5″, and the corresponding central density is 2.0×10^6 H_2 cm^{-3}. This model gives a maximum column density of 2.4×10^{23} H_2 cm^{-2} (without any convolution).

We assumed that the water abundance depends on the optical depth in the cloud due to the competition between depletion and photodissociation processes, according to the model presented in Bergin & Snell (2002) (see their Fig. 3). According to this model, the fractional H_2O abundance, $\chi(H_2O)$, increases to about 10^{-7} in the A_V range ∼2–4, and drops below 10^{-10} at higher extinctions. The radial distributions of the H_2 number density, A_V, and $\chi(H_2O)$ for our best-fit model are shown in Fig. 5. The H_2O column density in this model is $N(H_2O) = 3.4 \times 10^{14}$ cm^{-2}, and the average fractional abundance is $\langle\chi(H_2O)\rangle = 1.4 \times 10^{-9}$.

Using the model described above, we calculated H_2O spectra as observed with Odin. All radiative transfer calculations, including the dust temperature distributions and the H_2O line emission, were performed using our Monte Carlo program (Juvela 1997). The results of the line modelling are shown in Fig. 6. The 557 GHz line spectrum corresponding to the model presented in Fig. 5 is shown in the top panel of Fig. 6. The diagram in the bottom panel illustrates the effect of scaling of the Bergin & Snell (2002) abundances on the line peak intensity. On

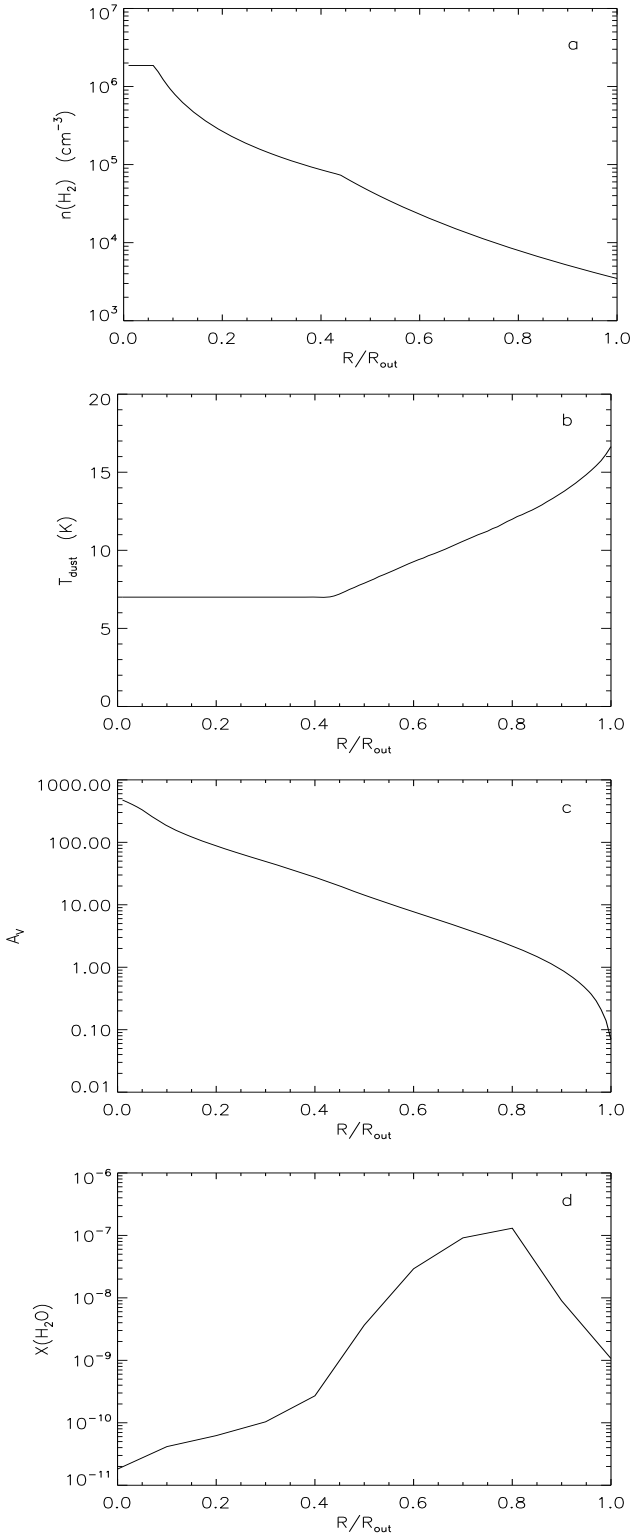

Fig. 5. Core model. The radial distributions of the gas density **a)**, temperature **b)**, visual extinction **c)** and the fractional H_2O abundance, $\chi(H_2O)$ **d)**. The dependence of $\chi(H_2O)$ on A_V is adopted from the model of Bergin & Snell (2002). The outer radius of the model is 230″, corresponding to 35 000 AU (0.17 pc).

the x-axis is a scaling factor with which the fractional abundance from the Bergin & Snell (2002) model has been multiplied. The scaling factor 1 corresponds to the average fractional abundance quoted above, i.e., $\langle\chi(H_2O)\rangle = 1.4 \times 10^{-9}$. Our detection limit

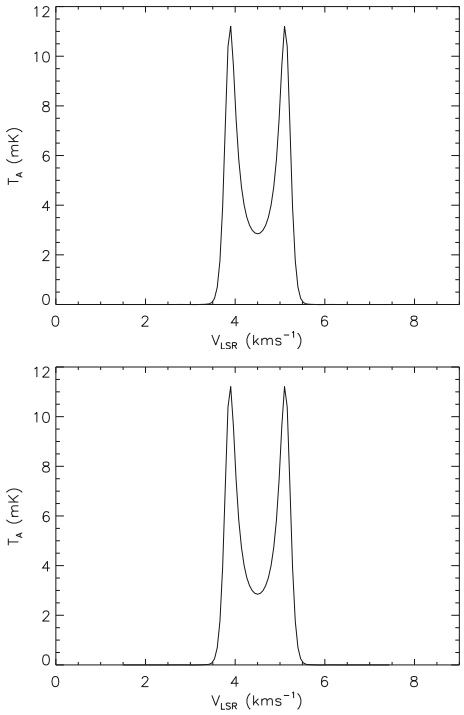

Fig. 6. *Top*: H_2O spectrum calculated from the model described in Sect. 5 and in Fig. 5. *Bottom*: expected peak antenna temperature of the 557 GHz H_2O line as a function of the scaling factor used to multiply the Bergin & Snell (2002) abundances. The detection limit (the dashed horisontal line) corresponds to a scaling factor of 5.

(16 mK) corresponds roughly to a factor of five with respect to this model. In other words, the non-detection is consistent with the Bergin & Snell (2002) model.

6. Discussion

The non-detection of the 557 GHz water line towards Cha-MMS1 is consistent with the core model derived from the 1.3 mm dust continuum observations with SIMBA, and the chemistry model of Bergin & Snell (2002) appropriate for quiescent cores. According to the adopted chemistry model, water is supposed to be nearly completely depleted in the cold, dense interiors of the core, and the possible line emission originates in the outer parts with moderate visual extinctions. Despite the relatively shallow emission region, the predicted line is optically thick and self-absorbed, which further hampers the detection. The average H_2O column density in the adopted core model is 3.4×10^{14} cm^{14} cm^{-2}, and the average fractional water abundance is 1.4×10^{-9}. Our calculations suggest that line detection with Odin would have required the average abundance to be at least five times higher.

One of the uncertainties of the model is the extend of the emission region. Judging from the fact that the SIMBA map is not sensitive to the large scale emission we added a pedestal of 2 MJy sr^{-1} to the core emission, but assumed that the density drops rapidly between the distances 150″ and 230″ from the core centre. To examine the validity of this assumption we inspected IRAS 100 μm emission maps, and the extinction maps derived from the 2MASS survey. These maps are not useful very close to Cha-MMS1, but they do show the full extent of the cloud. There is an area of ∼10′ around the core where the visual extinction is 5 mag or more ($N(H_2) \geq 5\,10^{21}$ cm^{-2}). Similarly, 100 μm emission at a distance of 5′ has an intensity of ∼30 MJy sr^{-1}. Extrapolation with the modified Planck funtion $B_\nu(T)\,\nu^2$ would give at 1.2 mm the intensity ∼1.0 MJy sr^{-1} for $T = 16$ K ($N(H_2) \sim 10^{21}$ cm^{-2}, assuming a mass absorption cross-section per unit mass of dust, $\kappa_{\nu,d}$, of 1 cm^2 g^{-1}, and a gas-to-dust ratio of 100). Based on what is said above, we think that the assumed extension of the core model to 230″ is a reasonable way to recognize the presence of the underlying, extended cloud. Probably it underestimates the amount of diffuse molecular gas encompassed by the beam, and therefore the derived upper limit for the average fractional water abundance is conservative.

Cha-MMS1 has been suggested to power a giant outflow with an extend of about 1 pc, associated with the Herbig-Haro objects HH 49, 50, 906, 922, and 925 on the southern side of the core, and HH 924 on its northern side (Bally et al. 2006). The absence of water line emission suggests that this outflow does not give rise any powerful shocks in the core. The situation is thus very different from the far-infared source IRAS 16293-2422 in Ophiuchus, where strong water lines have been detected towards the protostellar core and locations where the outflow interacts with surrounding dense material (Stark et al. 2004; Ristorcelli et al. 2005). IRAS 16293-2422 is supposed to be a Class 0/I transition object, whereas Cha-MMS1 is likely represent an earlier stage (Belloche et al. 2006). The fact that no CO outflow emanating from Cha-MMS1 has been detected conforms to the quiescent core model with no detectable water. Furhermore, unless an energetic jet can leave the core without any trace, it seems that the central source of the "giant outflow" lies somewhere else.

The blueshifted outflow from the nearby Class I protostar IRS4 seems to be directed towards Cha-MMS1 (Belloche et al. 2006; Hiramatsu et al. 2007), and lies almost entirely within the half-power beam of Odin. Water has been detected towards several protostellar outflows. Typically these objects show broad line wings with velocity ranges exceeding 20 km s^{-1} (e.g., Bergin et al. 2003; Stark et al. 2004; Franklin et al. 2007). In contrast, the CO "wing" emission near IRS4 is confined with 10 km s^{-1}, and no high-velocity shock tracers like SiO have been detected in this region (Hiramatsu et al. 2007). On the other hand, IRS4 has been suggested to drive the Herbig-Haro objects HH 49 and HH 50 some 10′ south of Cha-MMS1 (Hiramatsu et al. 2007). If this is true, the situation can be understood so that the high-velocity jet from IRS4 passes the Cha-MMS1 core. The claimed interaction (Hiramatsu et al. 2007) can occur between the expanding turbulent wake behind this jet and the core. In accordance with the models of Draine et al. (1983), the resulting low-velocity shock ($v < 10$ km s^{-1}) does not cause substantial erosion of the ice mantles of grains which would release oxygen into the gas phase. According to Hiramatsu et al., the mass of the blueshifted CO outflow is about 0.1 $M_\odot$. We estimate that detectable water signal from this component would require a fractional abundance of 3×10^{-6} or higher.

Finally, we note that the detection of the quiecent H_2O will be difficult even with Herschel/HIFI, despite a factor of ten better sensivity as compared with Odin. The predicted peak intensity (T_{MB}) of the 557 GHz line from our core model is 3.5 mK, as observed with Herschel/HIFI. That is about three times smaller than the predicted signal in the Odin beam. The low intensity is caused by the relatively small beam size (∼40″) of Herschel at this frequency, and the fact that most of the line emission comes from large distances from the core centre.

Acknowledgements. We thank Alain Lecacheux and Philippe Baron for very helpful discussions. We acknowledge support from the SGDO-CNES, and the Academy of Finland through grants 117206, 115056, and 124620.

References

Aikawa, Y., Herbst, E., Roberts, H., & Caselli, P. 2005, ApJ, 620, 330
André, P., Ward-Thompson, D., & Barsony, M. 1993, ApJ, 406, 122
Bally, J., Walawender, J., Luhman, K. L., & Fazio, G. 2006, AJ, 132, 1923
Belloche, A., Parise, B., van der Tak, F. F. S., et al. 2006, A&A, 454, L51
Bergin, E. A., & Melnick, G. J. 2005, in Astrochemistry: Recent Successes and Current Challenges, ed. D. C. Lis, G. A. Blake, & E. Herbst, Proc. IAU Symp., 231
Bergin, E. A., & Snell, R. L. 2002, ApJ, 581, L105
Bergin, E. A., Snell, R. L., & Goldsmith, P. F. 1996, ApJ, 460, 343
Bergin, E. A., Melnick, G. J., Stauffer, J. R., et al. 2000, ApJ, 539, L129
Bergin, E. A., Kaufman, M. J., Melnick, G. J., Snell, R. L., & Howe, J. E. 2003, ApJ, 582, 830
Draine, B. T., Roberge, W. G, & Dalgarno, A. 1983, ApJ, 264, 485
Harwit, M., Neufled, D. A., Melnick, G. J., et al. 1998, ApJ, 497, L105
Franklin, J., Snell, R. L., & Kaufman, M. J. 2007 [arXiv:0711.2055]
Giannini, T., Nisini, B., & Lorenzetti, D. 2001, ApJ, 555, 40
Goldsmith, P. F., & Langer, W. D. 1978, ApJ, 222, 881
Haikala, L. K., Harju, J., Mattila, K., et al. 2005, A&A, 431, 149
Hiramatsu, M., Hayakawa, T., Tatematsu, K., et al. 2007, ApJ, 664, 964
Hjalmarson, A., Frisk, U., Olberg, M., et al. 2003, A&A, 402, L39
Hollenbach, D. J. 1988, in Interstellar Matter, Proc. Second Haystack Observatory Meeting, ed. J. M. Moran, & P. T. P. Ho. (New York: Gordon and Breach Science Publishers), 39
Juvela, M. 1997, A&A, 322, 943
Knude, J., & Høg, E. 1998, A&A, 338, 897
Kontinen, S., Harju, J., Heikkilä, A., & Haikala, L. K. 2000, A&A, 361, 704
Lee, H.-H., Bettens, R. P. A., & Herbst, E. 1996, A&AS, 119, 111
Mattila, K., Liljeström, T., & Toriseva, M. 1989, in Low Mass Star Formation and Pre-Main Sequence Objects, ed. B. Reipurth, ESO Conf. Workshop Proc. 33, 153
Melnick, G. J., Stauffer, J. R., Ashby, M., et al. 2000, ApJ, 539, L77
Miettinen, O., Harju, J., & Haikala, L. K. 2006, A&A, 460, 721
Millar, T. J., Farquhar, P. R. A., & Willacy, K. 1997, A&AS, 121, 139
Neufeld, D. A., Lepp, S., & Melnick, G. J. 1995, ApJS, 100, 132
Neufeld, D. A., Snell, R. L., Ashby, M. L. N., et al. 2000, ApJ, 539, L107
Persi, P., Marenzi, A. R., Gómez, M., & Olofsson, G. 2001, A&A, 376, 907
Prusti, T., Clark, F. O., Whittet, D. C. B., Laurejs, R. J., & Zhang, C. Y. 1991, MNRAS, 251, 303
Reipurth, B., Nyman, L.-Å., & Chini, R. 1996, A&A, 314, 258
Ristorcelli, I., Falgarone, E., Schöier, F., et al. 2005, IAU Symp., 235, 227
Stark, R., Sandell. G., Beck, S. C., et al. 2004, ApJ, 608, 341
Snell, R. L., Howe, J. E., Ashby, M. L. N., et al. 2000a, ApJ, 539, L93
Snell, R. L., Howe, J. E., Ashby, M. L. N., et al. 2000b, ApJ, 539, L97
Snell, R. L., Howe, J. E., Ashby, M. L. N., et al. 2000c, ApJ, 539, L101
Spaans, M., & van Dishoeck, E. F. 2001, ApJ, 548, L217
Tennekes, P. P., Harju, J., Juvela, M., & Tóth, L. V. 2006, A&A, 456, 1037
Walmsley, C. M., Flower, D. R., & Pineau des Forêts, G. 2004, A&A, 418, 1035
Wilson, C. D., Mason, A., & Gregersen, E. 2003, A&A, 402, L59
Zinnecker, H., Krabbe, A., McCaughrean, M. J., et al. 1999, A&A, 352, L73